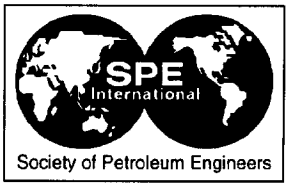

Ω

SPE 38728

High Resolution Reservoir Models Integrating Multiple-Well Production Data

Xian-Huan Wen, SPE, Clayton V. Deutsch, SPE, Stanford University, and A. S. Cullick, SPE, Mobil Upstream Strategic Research Center

Abstract

This paper presents a methodology to generate maps of high resolution permeability from multiple well single-phase flow rate and pressure data. The dynamic, i.e. temporal, production data contains important information about the interwell permeability distribuiton that should be integrated with static data, such as well and seismic data, to generate reservoir models to provide reliable input to reservoir simulation and reservoir management. A two-step procedure is proposed for such data integration: (1) establish the spatial constraints on large-scale permeability trends due to the production data using an inverse technique, and (2) construct the detailed geostatistical reservoir models subject to those spatial constraints using geostatistical techniques. The single-phase pressure and production data could be provided by permanent pressure gauges, simultaneous multiple well tests, or flow rates under primary depletion.

Production data and reservoir petrophysical properties, specifically permeability, are nonlinearly related through flow equations. Establishing the spatial constraints on permeability due to production data calls for the solution of a difficult inverse problem. This paper adapts the Sequential Self-Calibration (SSC) inverse technique to single-phase multiple-well transient pressure and rate data. The SSC method is an iterative geostatistically-based inverse method coupled with an optimization procedure that generates a series of coarse grid 2-D permeability realizations, whose numerical flow simulations correctly reproduce the production data. Inverse results using two synthetic data sets show this SSC implementation to be flexible, computationally efficient, and robust.

Fine-scale models generated by down-scaling the SSC generated coarse-scale models (using simulated annealing) are shown to preserve the match to the production data at the coarse-scale. Finally, reservoir performance prediction results show how the integration of production data can dramatically improve the accuracy of production forecasting with significantly less uncertainty.

Introduction

Optimal reservoir management requires reliable performance forecasts with as little uncertainty as possible. Incomplete data and inability to model the physics of fluid flow at a suitably small scale lead to uncertainty. Uncertainties in the detailed description of reservoir lithofacies, porosity, and permeability are large contributors to uncertainty in reservoir performance forecasting. Reducing this uncertainty can only be achieved by integrating additional data in reservoir modeling.

A large variety of geostatistical techniques have been developed that construct reservoir models conditioned to diverse types of static data including hard well data and soft seismic data.[6] Commonly, a number of techniques are applied sequentially to model the large reservoir geometry, the lithofacies, and then petrophysical properties such as porosity and permeability. However, conventional geostatistical techniques including Gaussian, indicator, annealing-based, or object-based methods are not suited to directly integrate dynamic production data.

Production data and reservoir petrophysical properties are related to each other through flow equations which are highly nonlinear. As a consequence, accounting for dynamic engineering data in geostatistical reservoir modeling is a difficult inverse problem.[8,9,11,14] Nevertheless, historical production data are often the most important information because they provide a direct measure of the actual reservoir response to the recovery process that form the basis for reservoir management decisions. Integrating dynamic production data is an important outstanding problem in reservoir characterization.

Ideally, we want to directly match all types of production data in the reservoir model at the required resolution simultaneously with other types of geological and geophysical data. A number of inverse techniques have been developed for this purpose.[2,8,10,11,12,13,15] Direct integration at the fine scale is not feasible because (1) the mathematical inversion of the flow equations is computationally intensive, (2) pressure and production data measured at the wells are responding to the spatial

variation of larger-scale effective properties, and (3) it is difficult to simultaneoulsly match production data with other static geological and geophysical data. Due to these limitations, currently available inverse techniques are limited to constructing relatively coarse scale models.

The coarse grid models that could be constructed by direct inversion techniques are usually inadequate for reliable production forecasting. In many practical situations, while keeping models as simple as possible, we would like to create highly-resolved models of lithofaces, porosity and permeability. Our proposal, therefore, is a two-stage approach where we (1) establish the spatial constraints on large-scale permeability trends due to the production data using an inverse technique , and (2) construct the detailed geostatistical models subject to those spatial constraints and the static data as well.

A review of available inverse techniques has been presented in reference [18]. In this paper, the Sequential Self-Calibration (SSC) inverse technique [9,17] is adapted to invert permeability distribution from multiple well, single-phase production data. Under the two-stage approach framework, the SSC method is considered as an interpretative tool of coding production data into spatial constraints of permeability (i.e., the multiple realizations of coarse grid permeability models) for the first stage (see Figure 1). An annealing-based geostatistical technique is used to construct high resolution reservoir models constrained to the SSC generated coarse grid models for the second stage. The application of the SSC method to synthetic data sets document the utility and robustness of the method in generating coarse-scale permeability models. The ability of using the coarse grid models to generate fine-scale permeability models that preserve the match of the production data is illustrated. Finally, the importance of integrating production data is illustracted by performing reservoir forecasts based on the constructed fine-scale reservoir models.

The Sequential Self-Calibration (SSC) Method

The available production data include pressure $p_i(t)$ and flowrate $Q_i(t)$ with time t at a number of wells $i = 1, ...n_w$ (n_w being the number of wells). Our goal is to find a set of permeability values for numerical cells in a reservoir model that matches the observed pressure data under the given flowrate conditions. This match is established by solving the single-phase, slightly compressible flow equation:

$$\nabla(\frac{kh}{\mu}\nabla p) + Q = hc\phi\frac{\partial p}{\partial t} \qquad (1)$$

where k is permeability, ϕ is porosity, μ is viscosity, h is the thickness of the reservoir, and c is formation compressibility. The closeness of the pressure match may be quantified by an objective function:

$$O = \sum_i \sum_t w(i,t)\left[p_i^{obs}(t) - p_i^{cal}(t)\right]^2 \qquad (2)$$

where $p_i^{obs}(t)$ and $p_i^{cal}(t)$ are the observed and numerically calculated pressure data at well i at time t, respectively; $w(i,t)$ is the weight assigned to the observed pressure data $p_i(t)$ according to its reliability (accuracy).

The SSC method is an iterative geostatistically-based method coupled with an optimization procedure.[1,9] Like most geostatistical approaches, the SSC method generates multiple equally-likely realizations of permeability fields honoring different types of available static and dynamic field data. The realizations honor a specified histogram and variogram as modeled from the field data and dynamic pressure data at multiple wells in the sense that the solution of the flow equation in each of the generated realizations matches the measured pressure values at the same well locations.

The unique aspects of the SSC method are (1) the concept of *master points* and (2) a perturbation mechanism based on kriging. We propose to extend the method for petroleum applications. As an overview, the method can be described by the following steps (see also Figure 2):

Construct initial realizations: Multiple, initial permeability realizations are created by conventional geostatistical techniques constrained to all static (hard and soft) data and the specified permeability histogram and variogram. Each realization is processed one at a time with the following steps.

Solve the flow equations for the current model using the specified boundary and production rate conditions. A block centered finite difference method with a direct matrix solver was used to solve the flow equations in this study.

Compare the observed and calculated pressure values at the available wells and at the given time. If the difference is smaller than a preselected tolerance value, this permeability realization is considered to honor the dynamic pressure data and the procedure stops. Otherwise, proceed to the next step.

Select master points and solve an optimization problem to find the optimal perturbations of permeability at the master point locations. The locations of the master points are randomly selected and the well locations having permeability data are automatically included as master points. The number of master points is about one master point per correlation range of the permeability variogram. The optimal perturbations minimize the difference between the observed and calculated pressures. The master point concept reduces the space of parameters to be optimized, which significantly improves the computational efficiency of the method.

Propagate the perturbation through the entire field by kriging the optimal perturbations determined for the master point locations. The permeability field is updated by adding the smooth perturbation field to the previous permeability field. The same variogram as used to generate initial models is used to propagate the permeability perturbations at master points. This preserves the original spatial variation patterns in the permeability field.

Loop back to **Solve the flow equations** until convergence. Typically, fewer than 20 iterations are required.

Sensitivity coefficients (derivatives of pressure with respect to the perturbation of permeability values) at all master point locations at each time step are needed when solving the optimization problem using gradient-based methods. The efficient calculation of sensitivity coefficients has received significant attention in the literature.[3,4,11,12] Appendix A presents an efficient way of obtaining the required sensitivity coefficients as part of the flow solution. A modified gradient projection method is then used to obtain the optimal perturbation values at the selected master locations by minimizing the objective function, which is outlined in Appendix B.

It should be noted that the application of the SSC method requires information on the distribution of permeability at the scale of the numerical grid (histogram and variogram). Also it assumes that the permeability variation in entire model is governed by a single histogram and a single variogram model, which may limit its application when the permeability variations in a reservoir are due to the mixture of multiple populations (e.g., controlled by multiple lithofacies or channel objects), or when there are discontinuous features such as faults, channels, or facies boundaries. Furthermore, there is no direct control on the reproduction of the variogram in the updated realizations. A posterior check is thus needed to ensure that the appropriate inverse results are obtained. Nevertheless, promising results have been obtained in groundwater hydrology using the SSC method with different heterogeneity features including the identification of non-multiGaussian features and high permeability flow channels.[16,17,19,20]

Application of the SSC Method

In this section, we evaluate the ability of the SSC method to generate 2-D coarse-scale maps of permeability from multiple well production data, using two synthetic examples. In each example, a reference permeability model is first constructed and then the dynamic pressure responses at a number of wells, due to changing flow rates, are obtained by flow simulation. Based on the dynamic flowrate and pressure data and information on the permeability variogram, the SSC method is used to invert for permeability fields that match the production data. The inverted permeability fields are then compared with the reference field to evaluate the capability of the SSC method. Note that the application of the SSC method assumes that the permeability field is spatially distributed following a single distribution function that can be inferred from field data. A prior model of the variogram must be assumed (or inferred) as well. We will show later that the inversion results are robust to variations in the assumed variogram.

Example 1 The first example is a 2-D, 4000 foot square domain, which is discretized into 25 × 25 grid cells of 160 feet × 160 feet. There is a high permeability (500 md) band connecting the lower-left corner and upper-right corner. The permeability in other areas is constant at 10 md (see Figure 3). There are four wells: W1 at the center of cell (5, 21), W2 at (21, 21), W3 at (5, 5), and W4 at (21, 5). The four boundaries are no-flow boundaries, porosity is assumed constant at 0.2, reservoir thickness is 100 feet, viscosity 0.2 cp, formation compressibility 10^{-6} 1/psi, and well radius 0.3 feet.

The imposed production rates and the corresponding pressure responses at the different wells were solved numerically and are shown in Figure 4. The reason for the different shut in times is to create some-well interference so that more information on spatial variations of permeability is contained in the production data. Sensitivity studies, too exhaustive for this paper, were performed with other production scenarios.

Based on the production and pressure data at the four wells, the SSC method was used to estimate the spatial distribution of permeability within the domain using the same discretization. Initially, a constant permeability with $Ln(K) = 2$ md was assumed at all cells, an anisotropic variogram with very long correlation length (8000 feet) in the 45 degree direction was assumed to be accessible from other information. The sensitivity of the inverted results to the selection of the anisotropy and initial permeability model will be demonstrated later.

After 20 iterations (about 5 minutes on a SGI workstation), the pressure responses in the updated permeability field converge to the reference pressure data. Figure 5 shows the resulting updated permeability field. The spatially connected high permeability band connecting wells W2 and W3 is clearly seen. Figure 6 shows the pressure values at the four wells computed from the initial uniform permeability field (bullets) and from the final updated permeability field (open circles) together with the true results from the reference field (solid lines). The pressure responses in the initial field deviate dramatically from the true values, due to the poor initial model; however, the permeability field updated by the SSC method accurately reproduces the true pressure data at all wells.

Considering the fact that, in practice, the correct permeability variogram is rarely known, the influence of variogram parameters on inverse results was investigated. Also, the sensitivity of the inverse results to the initial permeabulity values and the number of master points was studied separately. Figure 7 shows the inverse permeability fields using different variogram parameters (correlation range varying from 1000 to 8000 feet, and principle anisotropy direction varying from 20 to 70 degree) and different initial permeability values (ranging from $Ln(k) = 0.5$ to 10). In all cases, the high permeability band is always retrieved, indicating the robustness of the SSC method.

Example 2 In the first example, the production data were computed from coarse grid reference model and the SSC method was used to invert permeability fields on the same coarse grid. This would not usually be the situation in field applications. A more realistic test is to have the synthetic production data generated from simulation using a fine grid reference model. Then, the inversion technique is used to create coarse grid models, which are then used as spatial constraints for the construction of high resolution reservoir models (i.e., the two-stage approach, see Figure 1).

In the second example, a 4000 feet × 4000 feet 2-D square domain was discretized into 100 × 100 fine grid with cell size

of 40 feet × 40 feet. A reference permeability at this fine scale was generated using sequential Gaussian simulation (see Figure 8a). The mean and variance of $Ln(K)$ were 3.0 and 3.0, respectively. The variogram model used to generate this reference field was anisotropic spherical, with correlation ranges in the two principal directions of 1700 feet and 350 feet. A coarse grid model (20 × 20) scaled up by geometric averaging from the reference field is shown in Figure 8b. This scaled-up coarse grid model is later used for visual comparison with the inverse coarse grid results.

Three wells (W1, W2, and W3) located at the center of fine scale cells (58, 88), (13, 43) and (88, 33) produced oil with varying production rates, analogous to the first example, and the corresponding pressure responses are shown in Figure 9. Note that wells W2 and W3 were connected by relatively high permeabilities, whereas well W1 was located in a relatively low permeability region. Other parameters used in solving the flow equation for pressure on the fine (100 × 100) were the same as in Example 1.

The SSC method generated coarse grid (20 × 20) permeability realizations for which flow simulation matches the production data. Figure 10 shows three initial permeability realizations generated using the sequential Gaussian simulation (left), and the corresponding three updated realizations by the SSC method (right), respectively. The statistics of the reference coarse grid model (i.e., Figure 8b) are used for generating these realizations (i.e., mean and variance of $Ln(K)$ are 3.0 and 2.03, respectively; correlation lengths are 1800 feet and 400 feet in $X-$ and $Y-$ directions, respectively). We can see the large differences among the initial realizations all of which deviate significantly from the reference coarse grid model (shown at the bottom of the figure). However, the spatial variation patterns in the updated realizations are much closer to the reference field, yet the difference from realization to realization is much smaller compared to the initial realizations. Figure 11 shows the pressure responses computed from a typical initial realization and its corresponding updated permeability realization compared with the true pressure data. The true pressure response is reproduced with high accuracy by the updated field, whereas the initial field's pressure responses deviate significantly from the true data.

We generated 300 coarse-grid realizations using the SSC method, from which the ensemble mean and standard deviation fields were computed and compared with the 300 initial fields (Figure 12). The histograms of coarse grid permeability values at two selected locations A and B (see Figure 12) from the 300 initial and updated realizations are shown in Figure 13. Figure 12 shows the reduced standard deviation (i.e., uncertainty) from the updated fields, particularly in the areas around the wells. Even away from the wells, the updated fields have lower standard deviations (e.g., locations A and B in Figure 13.

Construction of Fine Scale Permeability Models

Using the SSC method, a series of equally-likely realizations of coarse grid permeability fields can be generated, all of which share the same histogram, variogram and production data. Usually, more detailed geostatistical models are required for flow simulation predictions of reservoir performance. In this section, we demonstrate the promise of the two stage approach to integrate production data, using the SSC results as the first stage. Constructing fine scale models that honor the coarse grid realizations is a problem of down-scaling.

Simulated annealing is one method that can construct fine scale permeability models based on the coarse grid realizations, as well as honor information on the histogram and variogram of fine scale permeability.[5] Our first approach was to use annealing and add a component to the objective function to represent the difference between the coarse grid permeability values and the power averages of fine scale permeabilities within the same coarse block, i.e.,

$$O_{mw} = \sum_{i=1}^{n_{coarse-grid}} \left[\overline{k}_v(\mathbf{u}_i) - \overline{k}_v^*(\mathbf{u}_i)\right]^2 \qquad (3)$$

where $n_{coarse-grid}$ is the number of blocks on coarse grid model, $\overline{k}_v(\mathbf{u}_i)$ is the inverse permeability value at coarse block $\mathbf{u}_i$, and $\overline{k}_v^*(\mathbf{u}_i)$ is the ω power average of fine grid permeability values within the coarse block $\mathbf{u}_i$, which is given as:

$$\overline{k}_v^*(\mathbf{u}_i) = \left[\frac{1}{N}\sum_{\mathbf{u}_i \in V} k(\mathbf{u}_i)^\omega\right]^{1/\omega}$$

where N is the number of fine grid within a coarse block V. Different fine grid permeability models can be constructed, each of which matches the corresponding coarse grid permeability realization.

Figure 14 shows two realizations of fine grid (100 by 100) permeability generated by this annealing technique and compared with the corresponding coarse grid (20 by 20) images from the SSC inversion in the second example. The histogram and variogram used to construct the fine grid models were taken from the fine grid reference model and geometric averaging ($\omega \to 0$) was used. Other types of data, e.g seismic data, could also be honored at this stage.

In order to check if the fine grid permeability models still reproduce the dynamic production data, the pressure responses at the wells were solved on the fine grid models of Figure 14. Figure 15 shows the results (open circles) compared to the true responses from the reference field (solid lines) and the responses from the coarse grid model (bullets). The pressure responses are closely reproduced in the annealing-based fine grid permeability models. This indicates the promise of the two stage geological coding approach to integrate production data.

An alternative and more sophisticated approach for constructing fine grid models using the coarse grid spatial representations is to compute local conditional distributions of coarse grid permeability at each coarse grid block as given in Figure 13, then use simulated annealing to construct fine grid models integrating these probability constraints of the coarse grid values.[7] Nevertheless, the simpler approach presented above may see more extensive use in practice.

Improvement of Performance Prediction From Production Data Integration

Finally, we demonstrate the importance of integrating production data by predicting the reservoir performance in Example 2 using two sets of fine scale (100×100) geostatistical models: one generated by the sequential Gaussian simulation not accounting for the production data, the other generated by simulated annealing accounting for the coarse-scale spatial representations derived from the production data as discussed previously. Two realizations of the second model are shown in Figures 14b,d. At 120 days, a water injection well located at the center of cell (50, 49) begins injecting water at constant rate of 20000 STB/day (see Figure 14). The three wells (W1, W2, and W3) are producing with constant pressure of 1000 psi.

The comparisons of predicted total produced oil and water cuts in three wells (W1, W2 and W3) from 30 realizations of both models are shown in Figures 16 and 17, respectively. The true results computed from the reference fine-scale model are plotted as the thick, light curves. It is evident that the reservoir models not conditioned to the production data overpredict oil production rates, and severely overpredict water cuts at W1, but underpredict water cuts at W2 and W3 with large uncertainty. When the production data are integrated, the predicted performance is much closer to the true results with significantly less uncertainty. The low permeability barrier in the reference find grid model between the injection well and W1 is not well captured in the inverse coarse grid models. Also the variogram distance between the injection well and W1 is larger than other well pairs, thus there are more permeability variations between these two wells. These may explain why the predictions in W1 are so much away from the true results compared to the results at W2 and W3.

Figure 18 shows the histograms of total oil production rates of the entire field (Figures 18a,b), as well as the water cuts at individual wells (Figures 18c-h) from 200 unconditioned and conditioned models when the injected water is at pore volume injected (PVI) of 1.0. The true values from the reference field are shown in the same figure by bullets. The accuracy and uncertainty of forecasting are large using the models in which production data are not integrated, whereas integrating production data shows significant improvement in forecasting results in terms of accuracy and uncertainty.

Conclusions

The SSC method appears flexible and computationally efficient for integrating single-phase multiple well pressure/rate data. It is well suited as an interpretive tool for extracting spatial representations (i.e., 2-D coarse grid models) from production data for the two-stage approach. Results from the synthetic examples further indicate that the two-stage approach has promise to integrate production data. Reservoir performance predictions show that the integration of production data can dramatically improve accuracy and reduce uncertainty of reservoir simulation predictions for reservoir management.

Extensive work is required to explore the limits of the SSC method and to establish the practical range of application. Ongoing research will investigate the integration of multiple phase production data and extentions of these methods to coarse-scale models with different lithofacies and to 3-D. A method of analyzing the degree of interference of production data from different wells may also be useful to guide the selection of production data used in the inversion to increase the computational efficiency.

Acknowledgments

We thank Mobil Oil Corporation for permission to present this work. Technical support from and discussions with Prof. J. R. Capilla and Prof. J. J. Gómez-Hernández at Polytechnic University of Valencia, Valencia, Spain, on the use of SSC method are greatly acknowledged.

Nomenclature

p	=	pressure, psi
t	=	time, day
k	=	permeability, md
ϕ	=	porosity
μ	=	viscosity, cp
h	=	thickness of reservoir, feet
c	=	formation compressibility, 1/psi
Q	=	production rate, STB/day
O	=	objective function
$\overline{k}_v$	=	coarse grid permeability from inversion, md
$\overline{k}_v^*$	=	power average of fine grid permeability, md
V	=	volume of coarse grid block
N	=	number of fine grid cells in a coarse block
ω	=	averaging power
α	=	amplitude factor for constraint interval
β	=	moving step in updating parameters
Δk	=	permeability perturbation, md
$\{S\}$	=	sensitivity coefficient vector
$[A]$	=	transmissibility matrix
$\{B\}$	=	right hand side of discretized flow equation
$[W]$	=	inverse covariance of observation errors
k_{krig}	=	kriging estimation of permeability, md
σ_{krig}	=	standard deviation of kriging estimation
n_m	=	number of master points
n_w	=	number of wells
n_t	=	number of time steps
n_w	=	number of wells

References

1. J. E. Capilla, J. J. Gómez-Hernández, and A. Sahuquillo. Stochastic simulation of transmissivity fields conditioning to both transmissivity and piezometric data, 2. demonstration in a synthetic case. *Journal of Hydrology*, 1997. in press.
2. L. Chu, M. Komara, and R. A. Schatzinger. An efficient technique for inversion of reservoir properties using iteration method. In *1996 SPE Annual Technical Conference and Exhibition Formation Evaluation and Reservoir Geology*, pages 193–208, Denver, CO, October 1996. Society of Petroleum Engineers. SPE Paper Number 36512.

3. L. Chu, A. C. Reynolds, and D. S. Oliver. Computation of sensitivity coefficients for conditioning the permeability field to well-test pressure data. *In Situ*, 19(2):179–223, 1995.
4. A. Datta-Gupta, D. W. Vasco, and J. C. S. Long. Sensitivity and spatial resolution of transient pressure and tracer data for heterogeneity characterization. In *1995 SPE Annual Technical Conference and Exhibition Formation Evaluation and Reservoir Geology*, pages 625–637, Dallas, TX, October 1995. Society of Petroleum Engineers. SPE Paper Number 30589.
5. C. V. Deutsch. *Annealing Techniques Applied to Reservoir Modeling and the Integration of Geological and Engineering (Well Test) Data.* PhD thesis, Stanford University, Stanford, CA, 1992.
6. C. V. Deutsch and A. G. Journel. *GSLIB: Geostatistical Software Library and User's Guide.* Oxford University Press, New York, 1992.
7. C. V. Deutsch and X. H. Wen. Integrating large-scale soft data by simulated annealing and probability constraints. In *Report 10, Stanford Center for Reservoir Forecasting*, Stanford, CA, May 1997.
8. G. S. Feitosa, L. Chu, L. G. Thompson, and A. C. Reynolds. Determination of reservoir permeability distributions from well test pressure data. In *1993 SPE Western Regional Meeting*, pages 189–204, Anchorage, Alaska, May 1993. Society of Petroleum Engineers. SPE Paper Number 26047.
9. J. J. Gómez-Hernández, A. Sahuquillo, and J. E. Capilla. Stochastic simulation of transmissivity fields conditional to both transmissivity and piezometric data, 1. The theory. *J. of Hydrology*, 1997. in press.
10. N. He, A. C. Reynolds, and D. S. Oliver. Three-dimensional reservoir description from multiwell pressure data and prior information. In *1996 SPE Annual Technical Conference and Exhibition Formation Evaluation and Reservoir Geology*, pages 151–166, Denver, CO, October 1996. Society of Petroleum Engineers. SPE Paper Number 36509.
11. J. L. Landa, M. M. Kamal, C. D. Jenkins, and R. N. Horne. Reservoir characterization constrained to well test data: A field example. In *1996 SPE Annual Technical Conference and Exhibition Formation Evaluation and Reservoir Geology*, pages 177–192, Denver, CO, October 1996. Society of Petroleum Engineers. SPE Paper Number 36511.
12. D. S. Oliver. Incorporation of transient pressure data into reservoir characterization. *In Situ*, 18(3):243–275, 1994.
13. A. C. Reynolds, L. Chu, and D. S. Oliver. Reparameterization techniques for generating reservoir descriptions conditioned to variograms and well-test pressure. In *1995 SPE Annual Technical Conference and Exhibition Formation Evaluation and Reservoir Geology*, pages 609–624, Dallas, TX, October 1995. Society of Petroleum Engineers. SPE Paper Number 30588.
14. A. Tarantola. *Inverse Problem Theory: Methods for Data Fitting and Model Parameter Estimation.* Elsevier, Amsterdam, The Netherlands, 1987.
15. D. W. Vasco, A. Datta-Gupta, and J. C. S. Long. Integrating field production history in stochastic reservoir characterization. In *1996 SPE Annual Technical Conference and Exhibition Formation Evaluation and Reservoir Geology*, pages 829–840, Denver, CO, October 1996. Society of Petroleum Engineers. SPE Paper Number 36568.
16. X. H. Wen. *Geostatistical Methods for Prediction of Mass Transport in Groundwater.* PhD thesis, Royal Institute of Technology, Stockholm, Sweden, 1995.
17. X. H. Wen. *Stochastic Simulation of Groundwater Flow and Mass Transport in Heterogeneous Aquifers: Conditioning and Problem of Scales.* PhD thesis, Polytechnic University of Valencia, Valencia, Spain, 1996.
18. X. H. Wen, C. V. Deutsch, and A. S. Cullick. A review of current approaches to integrate flow production data in geological modeling. In *Report 10, Stanford Center for Reservoir Forecasting*, Stanford, CA, May 1997.
19. X. H. Wen, J. J. Gómez-Hernández, J. E. Capillo, and A. Sahuquillo. The significance of conditioning on piezometric head data for predictions of mass transport in groundwater modeling. *Math. Geology*, 28(7):961–968, October 1996.
20. D. A. Zimmerman, C. L. Axness, G. de Marsily, M. G. Marietta, and C. A. Gotway. Some results from a comparison study of geostatistically-based inverse techniques. Sandia National Laboratories, Albuquerque, NM, 1995.

Appendix A: Calculation of Sensitivity Coefficients

Discretization of the flow equation (1) using an implicit scheme leads to the following equation in matrix notation:

$$[A]\{P\}^{t+1} = \{B\} \tag{A-1}$$

where $[A]$ is the transmissibility matrix which accounts for spatial and time discretizations, as well as boundary conditions, $\{B\}$ is the right hand side matrix that accounts for time discretization and flow boundary conditions. The solution of pressure at time $t+1$ is obtained by inverting matrix $[A]$, that is,

$$\{P\}^{t+1} = [A]^{-1}\{B\} \tag{A-2}$$

The sensitivity coefficients at time step $t+1$ can be calculated right after the pressure at time $t+1$ is obtained. The perturbation of parameter k_m can be written as:

$$[A]\frac{\partial\{P\}^{t+1}}{\partial\Delta k_m} + \frac{\partial[A]}{\partial\Delta k_m}\{P\}^{t+1} = \frac{\partial\{B\}}{\partial\Delta k_m}, \qquad m = 1,\ldots,n_m \tag{A-3}$$

where n_m is the total number of master points, thus,

$$[A]\frac{\partial\{P\}^{t+1}}{\partial\Delta k_m} = \frac{\partial\{B\}}{\partial\Delta k_m} - \frac{\partial[A]}{\partial\Delta k_m}\{P\}^{t+1}, \qquad m = 1,\ldots,n_m \tag{A-4}$$

Note that Equation (A-4) has the same form as Equation (A-1) and the matrix $[A]$ has just been inverted when solving for the pressure $\{p\}^{t+1}$. The sensitivity coefficients can be obtained at the same time step $t+1$ by simple matrix operations, that is,

$$s_{m,t+1} = \frac{\partial\{P\}^{t+1}}{\partial\Delta k_m} =$$

$$[A]^{-1}\frac{\partial\{B\}}{\partial\Delta k_m} - [A]^{-1}\frac{\partial[A]}{\partial\Delta k_m}\{P\}^{t+1}, \qquad m = 1,\ldots,n_m \tag{A-5}$$

The elements of matrices $\partial[A]/\partial\Delta k_m$ and $\partial\{B\}/\partial\Delta k_m$ can be directly computed from the expressions of elements in matrices $[A]$ and $[B]$.

The efficient calculation of sensitivity coefficients has received significant attention in the literature.[3,4,11,12]

Appendix B: Minimization of Objective Function

The objective function given in Equation (2) can be written in the following matrix form:

$$O(\{P^{cal}\}) = \sum_{t=1}^{n_t}\left(\{P^{cal}\}_t - \{P^{obs}\}_t\right)^T [W]_t \left(\{P^{cal}\}_t - \{P^{obs}\}_t\right) \tag{B-1}$$

where $\{P^{cal}\}_t = \{p^{cal}_{t,1}, p^{cal}_{t,2}, ..., p^{cal}_{t,n_w}\}$ and $\{P^{obs}\}_t = \{p^{obs}_{t,1}, p^{obs}_{t,2}, ..., p^{obs}_{t,n_w}\}$ are the numerically calculated and observed pressures at well $i = 1, ..., n_w$ and time $t = t_1, ..., t_n$. $[W]_t$ is the inverse covariance matrix of observation errors at time t. If pressure measurement errors at different wells are independent, $[W]_t$ is a diagonal matrix with the form of

$$[W]_t = \begin{bmatrix} w_{1,t} & & & \\ & w_{2,t} & & \\ & & \cdots & \\ & & & w_{n_w,t} \end{bmatrix}$$

Objective function (B-1) is a non-linear function of the model parameters we need to compute (i.e., the perturbations of permeability at master locations, $\{M\} = \{\Delta k_1, \Delta k_2, ..., \Delta k_{n_m}\}$). We linealize the objective function by approximating the pressure data by retaining its first order Taylor expansion, i.e.,

$$\{P^{cal}\}^1_t \approx \{P^{cal}\}^0_t + \frac{\partial\{P\}_t}{\partial\{M\}}\{M\} \tag{B-2}$$

where $\{S\}_t = \partial\{P\}_t/\partial\{M\} = \{s_{1,t}, s_{2,t}, ..., s_{n_m,t}\}$ is the sensitivity vector at time t with respect to the permeability perturbation at location m computed as presented in Appendix A, with $s_{m,t} = \partial\{P\}_t/\partial\{\Delta k_m\}$. $\{P^{cal}\}^0_t$ and $\{P^{cal}\}^1_t$ are pressure values at time t before and after introducing a perturbation matrix $\{M\}$. Using this linear approximation, after some manipulation, we can write our objective function (B-1) as following:

$$O(\{P^{cal}\}^1) = O(\{P^{cal}\}^0) + \sum_{t=1}^{n_t}\{D\}_t^T\{M\} + \sum_{t=1}^{n_t}\{M\}^T[C]_t\{M\} \tag{B-3}$$

where the elements of matrices $\{D\}_t$ and $\{C\}_t$ are expressed as follows:

$$d_{k,t} = 2\left(\{P^{cal}\}_t - \{P^{obs}\}_t\right)^T [W]_t\{S\}_t$$

$$c_{k_1k_2,t=} \left(\{S\}_t\right)^T [W]_t\{S\}_t$$

The constraints used for minimizing the objective function (B-3) are simply the possible minimum and maximum values of perturbations, i.e.,

$$\{\Delta k_{\min}\} \le \{M\} \le \{\Delta k_{\max}\} \tag{B-4}$$

i. e.,

$$\begin{matrix}[I]\{M\} \le \{\Delta k_{\max}\} \\ -[I]\{M\} \le \{\Delta k_{\min}\}\end{matrix} \tag{B-5}$$

where $[I]$ is a $n_m \times n_m$ identity matrix, $\{\Delta k_{\min}\} = \min\{K^0, K_{krig} - \alpha\sigma_{krig}\}$ and $\{\Delta k_{\max}\} = \max\{K^0, K_{krig} + \alpha\sigma_{krig}\}$. $\{K^0\}$ is the vector of permeability values at master points in the initial field, $\{K_{krig}\}$ and $\{\sigma_{krig}\}$ are kriging estimations and the corresponding kriging standard deviations at the master points based on available measured permeability data. If there is no prior K measurements, $\{K_{krig}\}$ and $\{\sigma_{krig}\}$ can be selected as the mean and standard deviation of the desired permeability histogram. α is a constant value that specifies the interval size of the constraints.

The above formulation is a standard quadratic optimization problem. In the current SSC code, we solve this optimization problem using a modified gradient projection method to take advantage of the simple expression of constraints expressed in equation (B-5). At each iteration of the optimization process, the search direction is obtained by projecting the gradient of the objective function on the null space of the gradients of the binding constraints (see reference 9 for details).

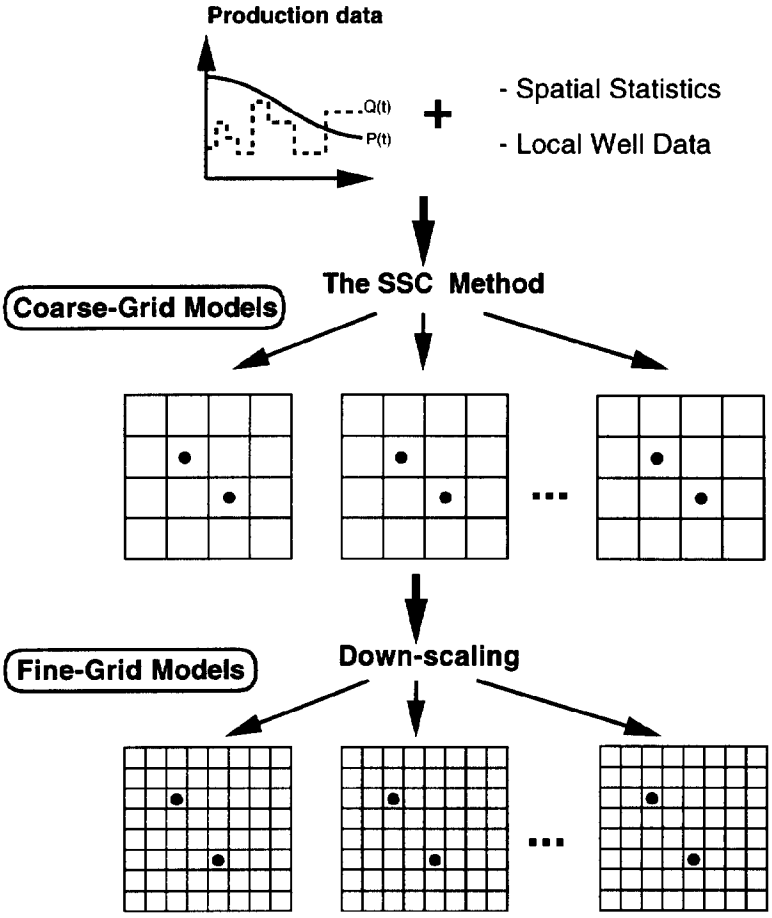

Figure 1: The Sequential Self-Calibration (SSC) method as an interpretative tool for the first stage under the two-stage approach framework. The second stage of constructing fine grid models accounting for the SSC generated coarse grid models is a down-scaling problem.

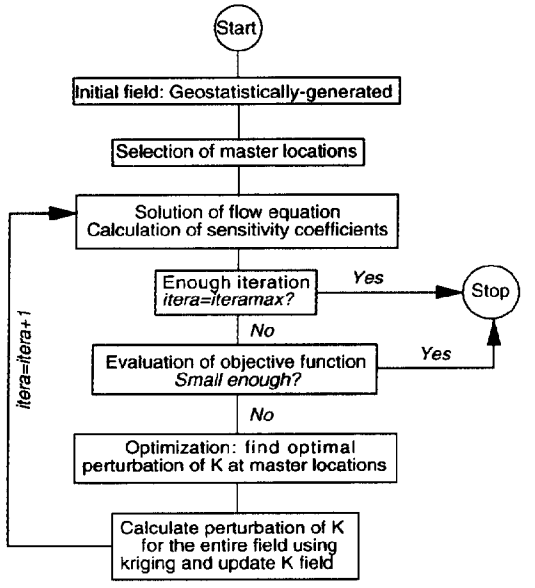

Figure 2: Flowchart of the Sequential Self-Calibration method.

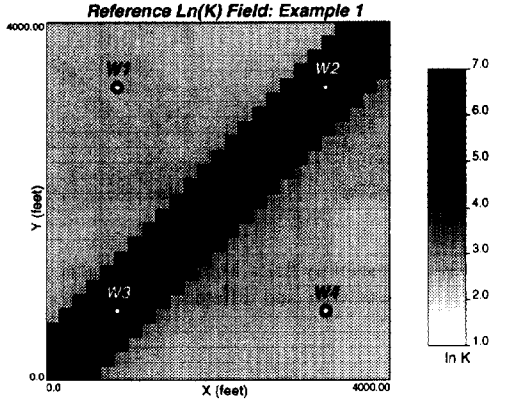

Figure 3: The reference deterministic permeability field: the first example.

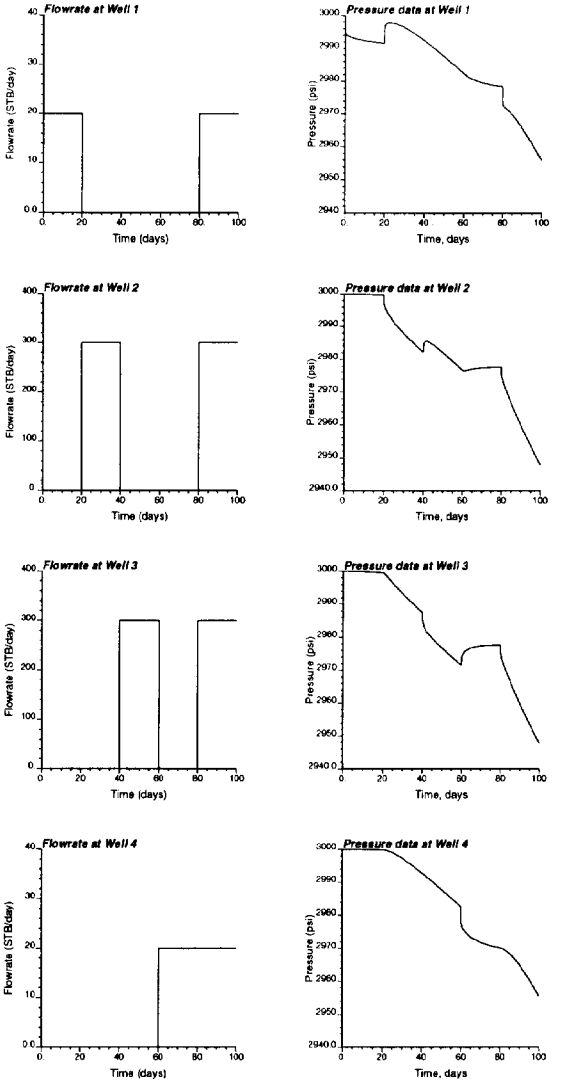

Figure 4: The production data (rates and pressures) obtained from the reference field: the first example.

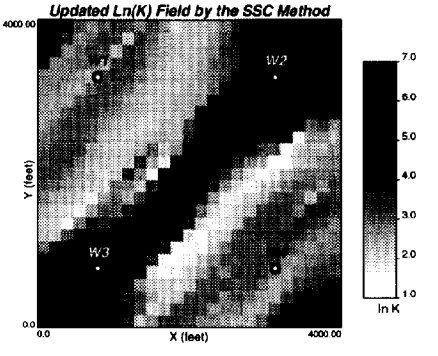

Figure 5: Final SSC-derived permeability field honoring pressure data from reference permeability field (see Figure 3).

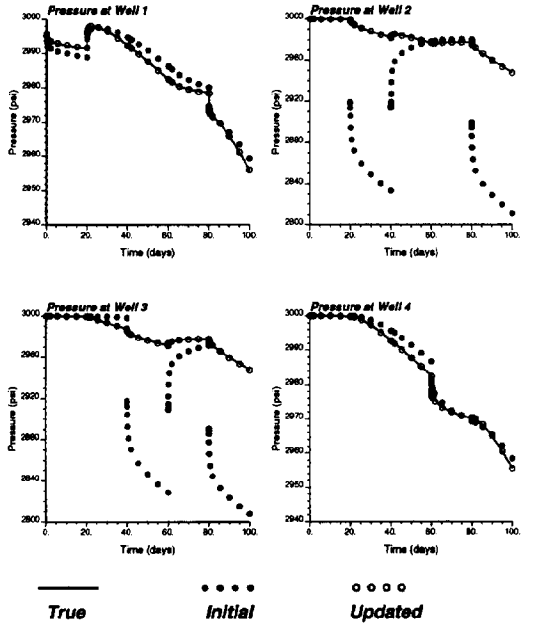

Figure 6: The pressure responses computed from initial (bullets) and updated (open circles) permeability fields together with the true data (solid lines): the first example.

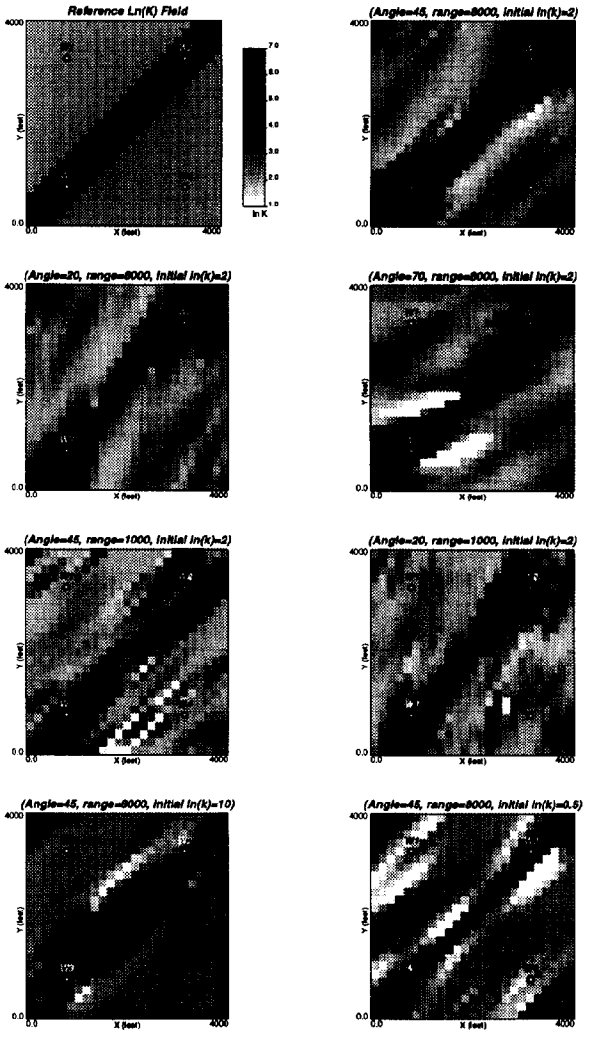

Figure 7: Inverse permeability fields from the SSC method by using different variogram parameters and different initial values: the first example.

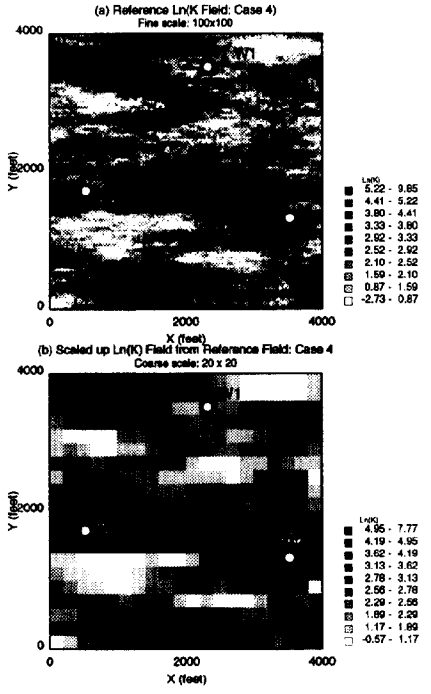

Figure 8: (a) The reference permeability field at fine scale, and (b) and the scaled up coarse grid permeability model: the second example.

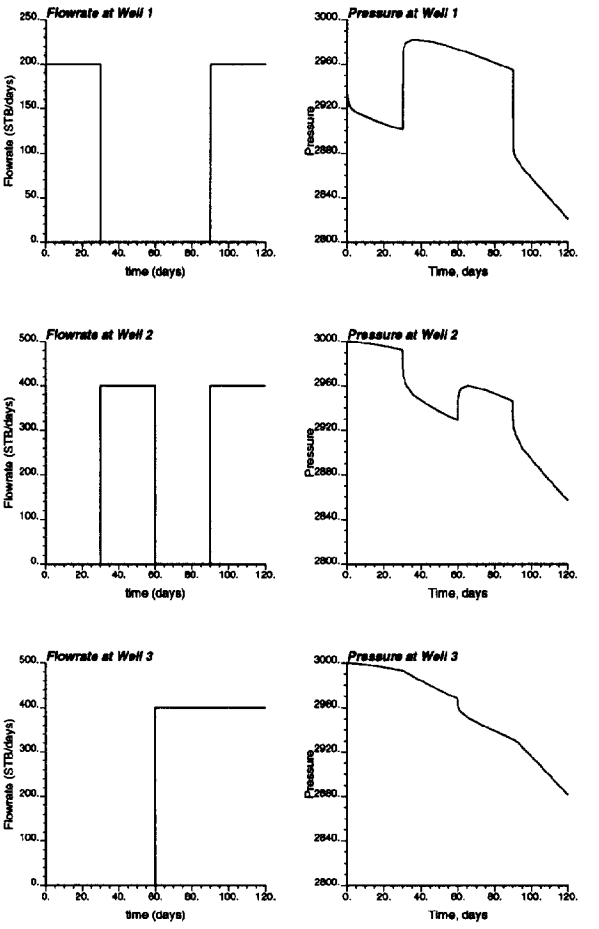

Figure 9: The production data (rates and pressures) obtained from the reference field at fine scale: the second example.

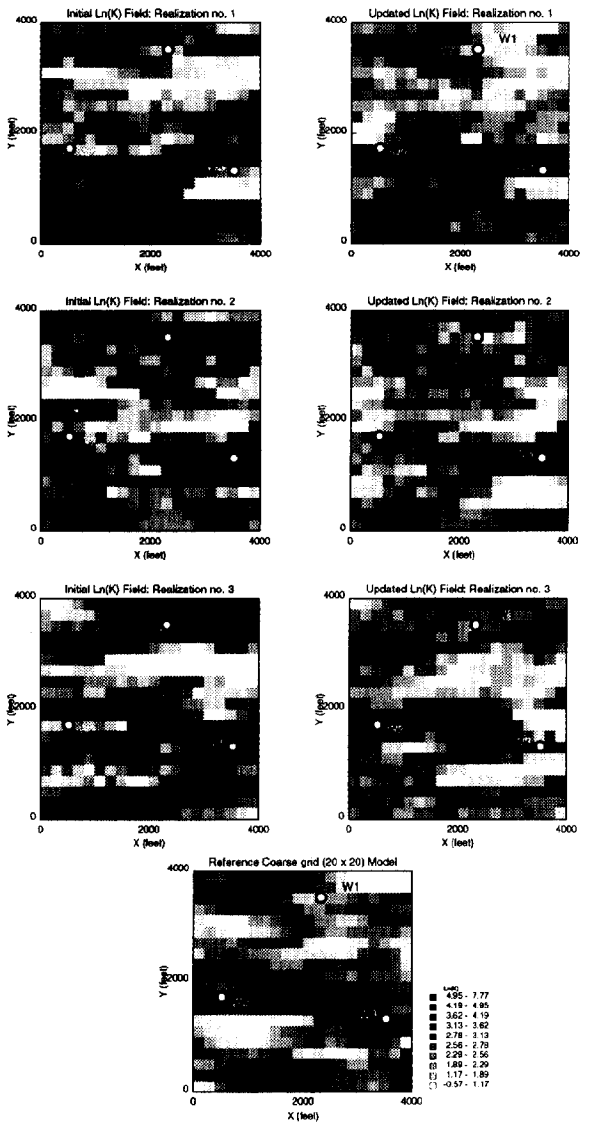

Figure 10: Three initial permeability realizations and the corresponding updated fields from the SSC method.

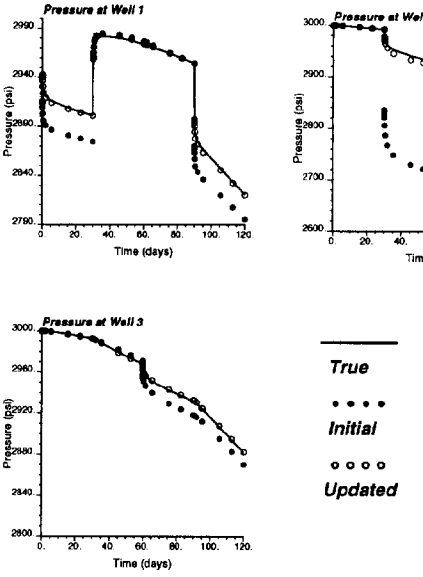

Figure 11: The pressure responses computed from the typical initial and updated permeability fields together with the true data in a typical realization: the second example.

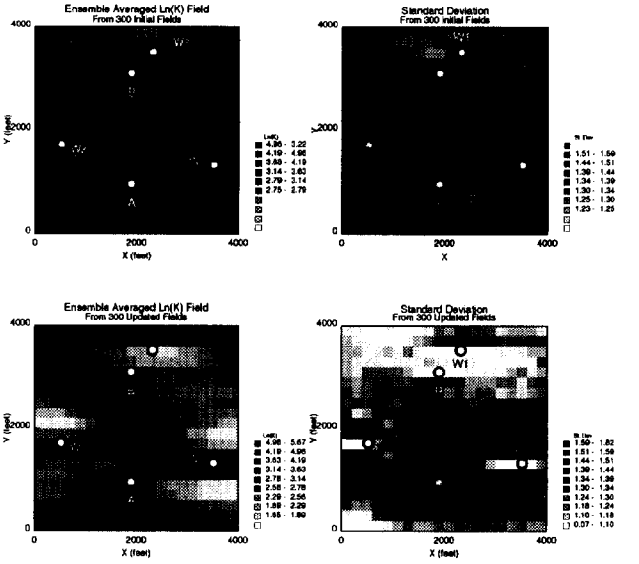

Figure 12: The ensemble averaged permeability field and the corresponding standard deviations from 300 initial and updated realizations: the second example.

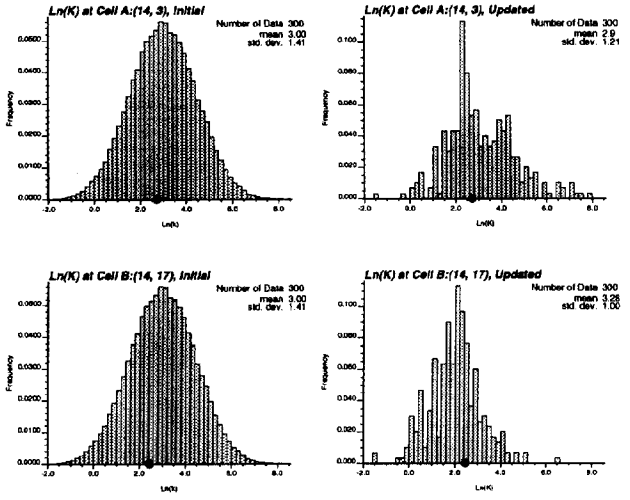

Figure 13: The histograms of coarse grid permeability values at locations A and B (see Figure 12) computed from 300 initial and updated realizations: the second example. The bullets are the values from the reference coarse field at the same locations.

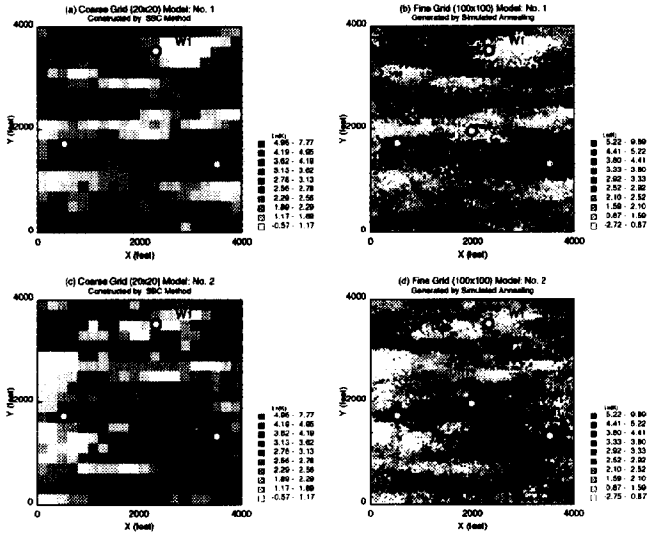

Figure 14: Two realizations of fine grid models, constructed by the simulated annealing method, that honor the coarse grid models generated by the SSC method shown on the left-hand side.

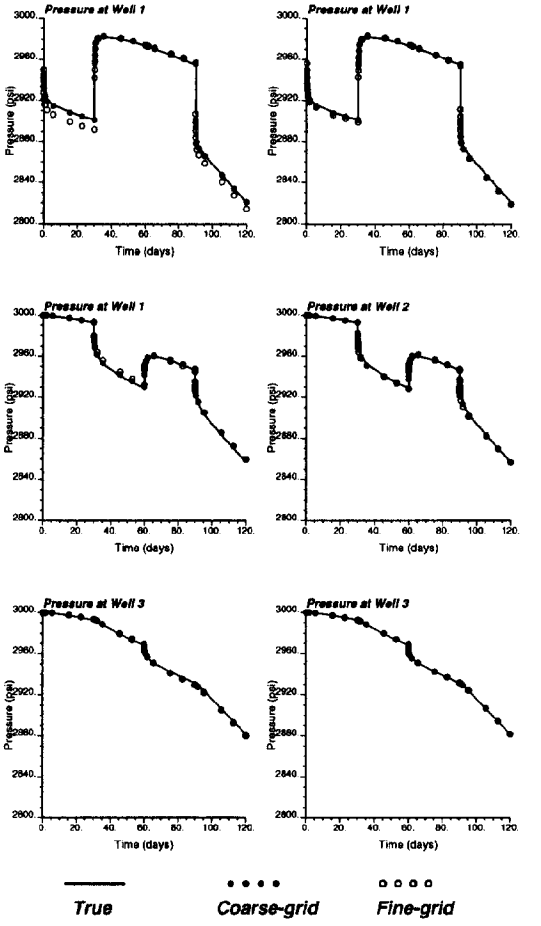

Figure 15: The comparison of pressure responses computed from fine and coarse grid models shown on the top of Figure 14 to the true results.

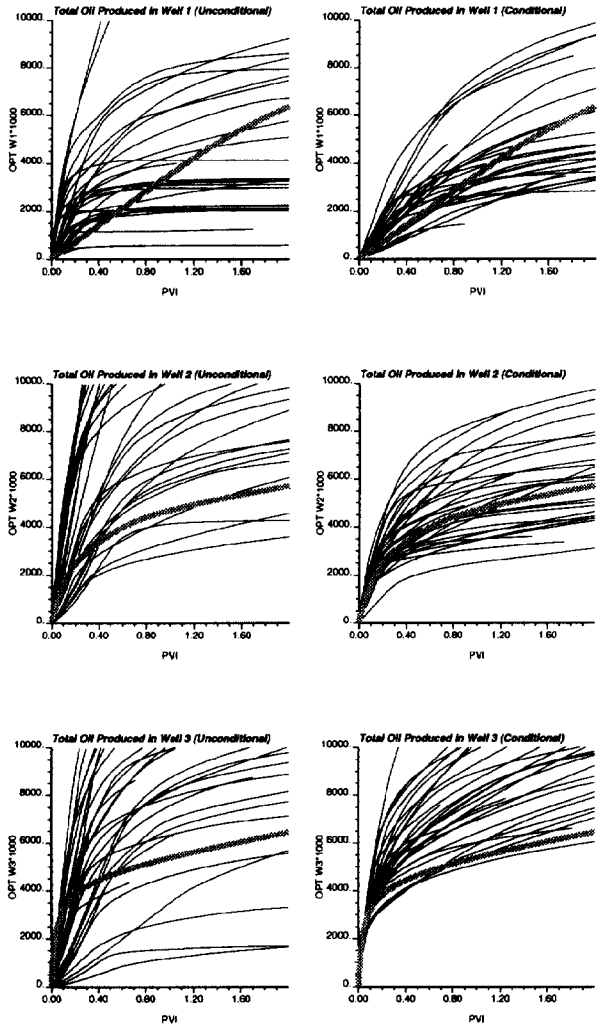

Figure 16: The total oil production rates at the producing wells from 30 unconditioned (left) and conditioned (right) realizations. The thick light curves are results from the reference true field.

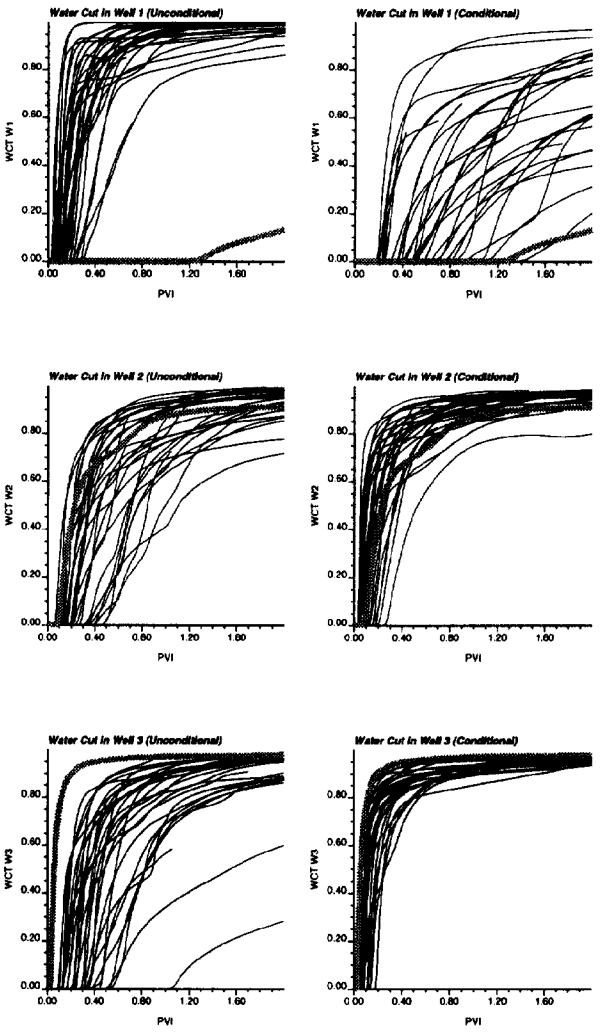

Figure 17: The water cuts at the producing wells from 30 unconditioned (left) and conditioned (right) realizations. The thick light curves are results from the reference true field.

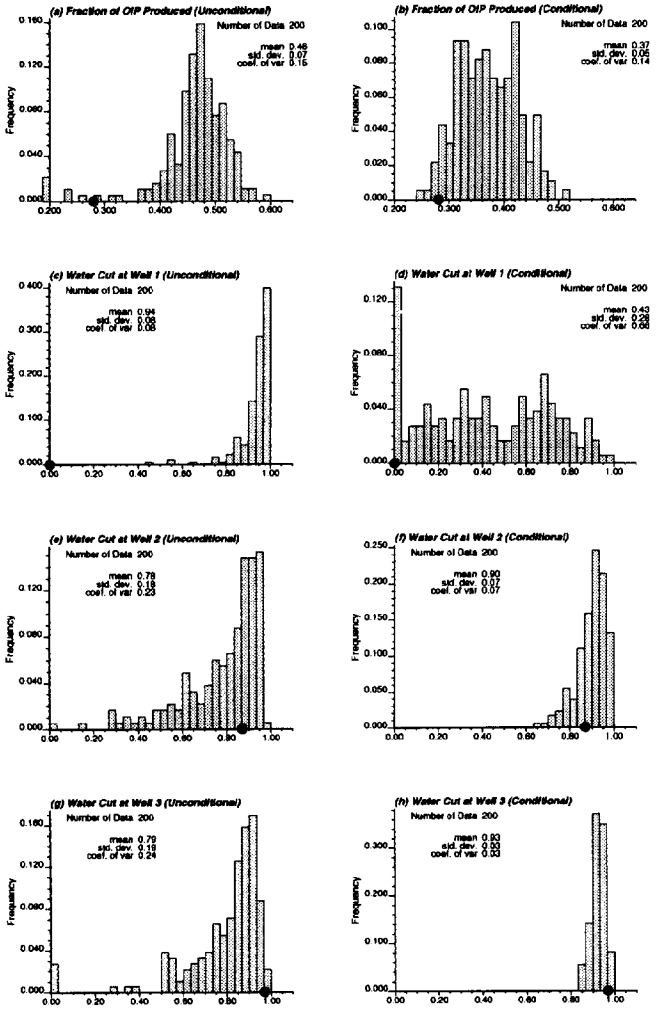

Figure 18: The histograms of total oil produced (a, b) and water cuts at three wells (c-h) from 200 unconditioned (left) and conditioned (right) realizations when the injected water is at $PVI = 1.0$. Bullets are the true results from the reference field.